LANGMUIR

pubs.acs.org/Langmuir Article

Solvent-Mediated Forces between Ellipsoidal Nanoparticles Adsorbed at Liquid−Vapor Interfaces

Olav Galteland,* Fernando Bresme, and Bjørn Hafskjold

Cite This: https://dx.doi.org/10.1021/acs.langmuir.0c02243 Read Online

ACCESS | Metrics & More | Article Recommendations | Supporting Information

ABSTRACT: Classical capillary theory predicts that a non-neutrally wetting ellipsoidal particle adsorbed at a liquid−vapor interface will deform the interface. The deformation gives rise to anisotropic capillary forces of a quadrupolar nature that induce strong directionality in the particle interactions. Here, we investigate the interactions between nanoparticles with characteristic lengths of 1−5 nm. We show that the near-field interactions are dominated by solvent-mediated forces, which arise from the fluid packing between the nanoparticles and direct nanoparticle−nanoparticle interactions. The solvent-mediated forces are two orders of magnitude larger than the estimated capillary force. We find that interacting ellipsoidal nanoparticles adsorbed at the liquid−vapor interface have a larger repulsion in the depletion region than the nanoparticles submerged in a dense bulk phase and argue that this is because of a negative line tension associated with the three-phase line.

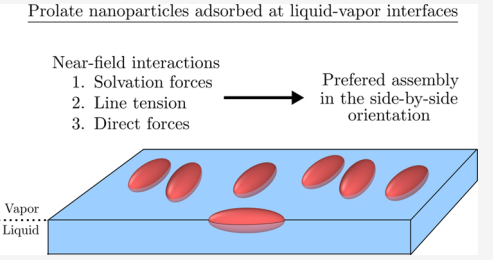

INTRODUCTION

The interaction between nanoparticles and fluid interfaces is important in a wide range of technological applications concerned with paint, powders, dispersions, or suspensions, as well as in fundamental problems related to capillary phenomena.[1] New materials can be created via the self-assembly of nanoparticles adsorbed at interfaces.[2,3] These approaches take advantage of the strong adsorption energies of particles at liquid−vapor and liquid−liquid interfaces.[1] Large spherical particles (radius larger than 5 μm) will deform the interface[4] because of their weight. The deformation induces attractive forces, so-called flotation forces, between particles. Perfectly spherical particles, much smaller than the capillary length, sub-micrometer sizes, do not deform the interface to an appreciable extent, and therefore, they will not induce flotation forces. However, particle anisotropy can induce interfacial deformations when the particles are non-neutrally wetting. In particular, ellipsoidal particles adsorbed at fluid interfaces induce quadrupolar deformations, which lead to orientation-dependent lateral capillary forces.[5,6] The side-by-side (SS) and tip-to-tip (TT) orientations are attractive, while the side-to-tip (ST) is repulsive. As a result, ellipsoidal particles can agglomerate in open structures, such as chains.[7,8]

The strength of such quadrupolar forces changes with the particle size. It is expected that in the nanoscale regime these interactions can become of the order of k_BT; hence, other interactions may be important, particularly depletion interactions corresponding to particle distances on the order of the characteristic nanoparticle size or smaller. Solvent-mediated forces, which arise from the modification of the structure of the solvent confined between the nanoparticles, are expected to be important at the nanoscale. Indeed, Bresme *et al.* calculated the solvent-mediated forces between the spherical nanoparticles adsorbed at liquid−vapor interfaces using molecular dynamics simulations.[9] They found that the solvent-mediated forces oscillate with a period equal to the fluid particle diameter and the forces are different for particles at interfaces and particles in bulk, fully immersed in either the vapor or liquid phase. Evidence for line tension contributions at interparticle distances corresponding to the depletion region was also provided. Experimental evidence for line tension effects in nanoparticles and droplets were discussed extensively in a recent work,[10] while, to the best of our knowledge, the line tension effects in the depletion region have not been investigated yet experimentally.

In this work, we study interactions between the ellipsoidal particles adsorbed at the liquid−vapor interface in the near-field regime, when the distance between particles is of the order of a few solvent molecular diameters. We distinguish between three different interactions, solvent-mediated, capillary, and direct. The solvent-mediated interactions arise from the fluid packing between the nanoparticles, where the capillary interactions are due to deformations of the liquid-vapor interface and direction interactions between two nanoparticles. The solvent-mediated and capillary interactions are calculated together in our molecular simulations. The

Received: July 30, 2020
Revised: November 11, 2020

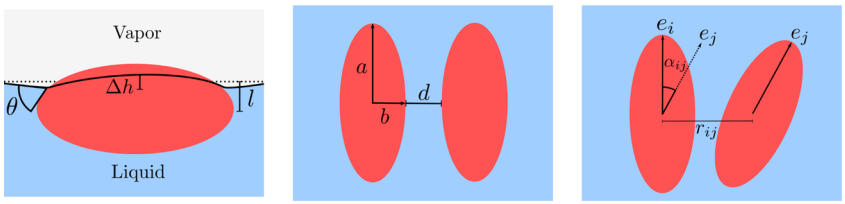

Figure 1. (a) Illustration of a non-neutrally wetting ellipsoidal particle adsorbed at a liquid−vapor interface, showing the interfacial deformation around the particle. Δh is the height difference between the highest and lowest points of the liquid−vapor interface around the nanoparticle, and θ is the contact angle of the liquid−vapor−nanoparticle interfaces. (b,c) Top-down view of two ellipsoidal particles adsorbed at a liquid−vapor interface. The relative orientations of the particles are represented by $\mathbf{e}_i$ and $\mathbf{e}_j$. r_{ij} is the distance between their centers of mass and $\cos \alpha_{ij} = \mathbf{e}_i \cdot \mathbf{e}_j$, where α_{ij} is the angle between $\mathbf{e}_i$ and $\mathbf{e}_j$. The major and minor axes of the ellipsoid is a and b, respectively, and d is the surface-to-surface distance between the particles.

analysis of the solvent-mediated interactions is not possible with the existing continuum approaches (see, *e.g.*, Dasgupta *et al.*[6]) because a continuum approach ignores solvent-mediated effects. To quantify the interactions, we use instead molecular simulations including the solvent at atomistic level explicitly. Our work, therefore, addresses the question on how relevant capillary forces are in ellipsoidal nanoparticles adsorbed at the interfaces.

Our paper is structured as follows. First, we define the theoretical background, the simulation model, and the numerical method used to perform our study. A discussion of the main results obtained follows. We close the article highlighting the main conclusions arising from our work.

MODEL AND METHODS

We have performed atomistic simulations to compute the interactions between ellipsoidal nanoparticles adsorbed at liquid−vapor interfaces. The nanoparticles are prolate ellipsoids, with one radius larger than the other two, $a > b = c$. The aspect ratio is defined as the large radius divided by the smaller, $\kappa = a/b = a/c$. The large radius studied in this work ranges from 0.3 to 1 nm and the aspect ratio κ ranges from 1 to 3. The fluid−fluid and fluid−nanoparticle interactions were modeled using the Lennard−Jones and the Gay−Berne potentials, respectively.[11] Direct nanoparticle−nanoparticle interactions were not included. Further details on the models and simulations are given below.

The work associated with moving a nanoparticle from the vapor phase to the liquid−vapor interface is given by the change in Helmholtz free energy[1]

$$\Delta F = (\gamma_{nl} - \gamma_{nv})A_{nl} - \gamma_{lv}A_{st} + \tau L \quad (1)$$

where A_{nl} is the area of the nanoparticle−liquid interface, A_{st} is the area of the liquid−vapor interface removed by the nanoparticle, $\gamma_{\alpha\beta}$ is the surface tension between phase α and β, and τ is the line tension of the three-phase line, of length L, where the particle and the two coexisting phases meet.

Non-neutrally wetting (contact angle $\theta \neq 90°$) ellipsoidal particles adsorbed at a liquid−vapor interface deform the interface. The deformations have a quadrupolar symmetry, with the liquid phase being pushed down at the tips of the particle and pulled up at the sides of the nanoparticle for contact angles $\theta < 90°$ and conversely for contact angles $\theta > 90°$ (see Figure 1a).

The lateral capillary forces between two identical particles i and j with a center-to-center separation r_{ij} and orientations described by the unit vectors $\mathbf{e}_i$ and $\mathbf{e}_j$ (see Figure 1c) are given by[5]

$$f_{ij}^{cap}(r, \alpha) = -12\pi\gamma_{lv}\cos(2\alpha_{ij})(\Delta h)^2\frac{b^4}{r_{ij}^5} \quad (2)$$

where $\cos \alpha_{ij} = \mathbf{e}_i \cdot \mathbf{e}_j$, Δh is the height of the interface deformation, as shown in Figure 1a, and b is the short axis of the ellipsoidal particle. For $\alpha_{ij} = \pi/2$, the capillary force is repulsive, and for $\alpha_{ij} = 0$ or π, it is attractive. This corresponds to the ST orientations being repulsive, while SS and TT orientations are attractive. The height of the interface deformation, Δh, depends on the contact angle and the particle size via b. The height, Δh, increases with increasing b and reaches a maximum at $\theta \approx 50°$, while $\Delta h = 0$ at $\theta = 90°$. For a nanoparticle with aspect ratio $\kappa = 3$ and contact angle $\theta \approx 50°$, the height of the interface deformation is approximately $\Delta h \approx 0.17b$, as predicted by the theoretical approach developed by Lehle *et al.*[5] This estimate is expected to slightly overestimate the deformation as compared with the values obtained using finite element calculations (see ref 12 for a comparison of theoretical and numerical calculations).

The capillary forces decrease with decreasing particle size. The characteristic size for these interactions to become of the order of the thermal energy (k_BT) was estimated in ref 12. The capillary interactions are expected to reach the thermal energy for sizes <10 nm. As noted in that work, below this size, the depletion entropic forces may become relevant. This idea is consistent with the numerical results reported in our work.

In order to study the details of effective interactions, we performed molecular dynamics simulations of nanoparticles adsorbed at a liquid−vapor interface in the canonical ensemble, using a Nosé−Hoover thermostat.[13] All the trajectories were generated with LAMMPS.[14]

The fluid−fluid interactions were modeled using the truncated and shifted Lennard−Jones potential

$$u_{ij}^{LJ}(r) = \begin{cases} 4\varepsilon_{ij}\left[\left(\frac{\sigma_{ij}}{r}\right)^{12} - \left(\frac{\sigma_{ij}}{r}\right)^{6}\right] - u_{ij}^{'LJ}(r_{c,ij}) & \text{if } r < r_{c,ij} \\ 0 & \text{else} \end{cases} \quad (3)$$

where ε_{ij} is the interaction strength, σ_{ij} is the fluid particle diameter, r is the center-to-center distance between particles, $r_{c,ij}$ is the cutoff distance, and $u_{ij}^{'LJ}(r_{c,ij})$is the interaction strength of the Lennard−Jones potential at the cutoff. The fluid−fluid interaction strength was set to ε_{ff}, the fluid particle diameter to σ_{ff}, and the cutoff distance to $r_{c,ff} = 2.5\sigma_{off}$. The fluid−nanoparticle interactions were modeled using a generalized Gay−Berne potential[15]

$$u_{ij}^{gb}(A_i, r_{ij}) = u_r(A_i, r_{ij})\eta(A_i)\chi(A_i, r_{ij}) \quad (4)$$

The factor u_r includes the distance-dependent interactions. It has the form of a 12−6 Lennard−Jones potential with a hard-core radius and a Lennard−Jones shell outside the hard-core. The factors η and χ include the dependence of the interaction strength with the relative orientation and position of the ellipsoids. A_i is the rotational matrix that describes the orientation of the ellipsoid. See the work by Evaraers and Ejtehadi[15] for details on the Gay−Berne potential. The direct nanoparticle−nanoparticle interaction was not included in this work, but a discussion of its relevance is given in the Supporting Information.

https://dx.doi.org/10.1021/acs.langmuir.0c02243
Langmuir XXXX, XXX, XXX−XXX

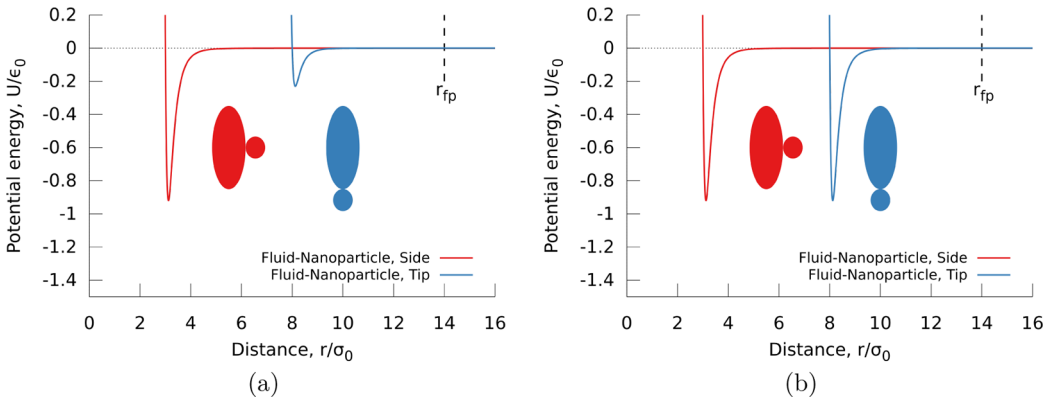

Figure 2. Potential energy between a fluid particle and a nanoparticle modeled with the Gay–Berne potential of radii $a = 7.5\sigma_0$, $b = c = 2.5\sigma_0$, with interaction strength $\varepsilon_{fp} = 3\varepsilon_0$ and well depth ratio (a) $\kappa' = 5$ and (b) $\kappa' = 1$. The dashed vertical lines show the cutoff distance for the fluid particle–nanoparticle interactions.

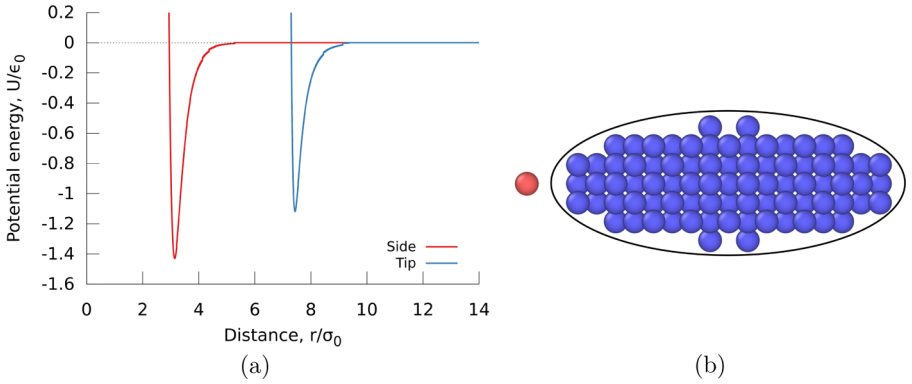

Figure 3. (a) Pair potential between a nanoparticle made up of Lennard–Jones atoms and a fluid particle in the tip and side orientations. (b) Ellipsoidal nanoparticle made up of Lennard–Jones atoms in blue and a fluid particle in red. The superimposed elliptical line illustrates the shape of the nanoparticle of radii $a = 7.5\sigma_0$, $b = c = 2.5\sigma_0$.

The generalized Gay–Berne potential makes it possible to model an ellipsoidal particle in terms of three principal axes with radii a, b, c and three different interaction strengths along each radius $\varepsilon_{a,i}$, $\varepsilon_{b,i}$, $\varepsilon_{c,i}$. The three radii a, b, c is the sum of a hard-core radius and a Lennard–Jones shell. The Lennard–Jones shell distance parameter is, in all cases, equal to the fluid diameter σ_0, while the hard-core radius is varied. In this work, we considered two particle shapes, namely, prolate particles with $a > b = c$ and spherical particles with $a = b = c$. We also simulated two cases corresponding to different nanoparticle interaction strengths: $\varepsilon_a = \varepsilon_b = \varepsilon_c = \varepsilon_0$ and $\varepsilon_a = 0.2\varepsilon_0$, $\varepsilon_b = \varepsilon_c = \varepsilon_0$. The well depth ratio is defined $\kappa' = \varepsilon_b/\varepsilon_a$. Figure 2 shows the potential energy between the fluid and the nanoparticle, see eq 4, for the side and tip interactions for (a) $\kappa' = 5$ and (b) $\kappa' = 1$ with the interaction strength $\varepsilon_{fp} = 3\varepsilon_0$. The well depth ratio $\kappa' = 5$ is a common choice for the Gay–Berne potential.[16,17] It is shown by Babadi *et al.*[18] that κ' ranging from 1 to 18 is a good choice as a coarse-grained model for some prolate and oblate mesogens.

The pair potentials, as represented in Figure 3a, show the interactions between a fluid particle and an ellipsoidal nanoparticle made up of particles interacting with the Lennard–Jones potential as defined in eq 3, as shown in Figure 3b. The attraction between the fluid particle and the nanoparticle is stronger on the side of the nanoparticle compared to the tips because the fluid particle is within the cutoff range of more particles at the side compared to the tip of the nanoparticle. This further suggests that the ellipsoidal model described above is a reasonable model for molecular nanoparticles.

A liquid–vapor interface was created from a face-centered cubic lattice of LJ atoms at a density $\rho^* = N\sigma_0^3/V = 0.8$. The temperature of the system was set to $T^* = k_BT/\varepsilon_0 = 2.0$ to generate a supercritical fluid phase. The system was run for 5×10^3 steps, using a time step of $\delta t^* = 0.002$ in reduced units for time, $t^* = \frac{t}{\sigma_0}\sqrt{\frac{\varepsilon}{m}}$. Following the equilibration, the temperature of the system was reduced to a subcritical temperature, $T^* = 0.7$, and the simulation box was extended with vacuum on either side of the liquid in the z-direction. The new total density was $\rho^* = 0.4$. The liquid–vapor two-phase system was equilibrated during 1.5×10^4 *NVT*-steps. The coexisting liquid and vapor densities were $\rho_l^* = 0.7896 \pm 0.0004$ and $\rho_v^* = (2.5 \pm 0.6)\times10^{-4}$, respectively, in good agreement with previous simulations.[19] The interfacial width (defined in eq 6) was $w = (2.231 \pm 0.004)\sigma_0$. The liquid–vapor surface tension for this system was found to be $\gamma_{lv}^* = \gamma_{lv}\sigma_0^2/\varepsilon 0 = 0.602 \pm 0.014$, which was calculated with the Irving–Kirkwood formula using the pressure tensor components[20]

$$\gamma_{lv} = \int_{z_l}^{z_v} (P_N(z) - P_T(z))dz \tag{5}$$

Here, z_l and z_v are positions in the bulk liquid and vapor phases and P_N and P_T are the normal and tangential components, respectively, of the pressure tensor.

We quantify the wettability of the nanoparticle using l/b, where l is the distance from the particle center to the liquid–vapor interface, defined by the Gibbs dividing surface (GDS) (see Figure 1a). The GDS is the position where the surface excess density is zero. It is found by fitting the parameters of the density profile, $\hat{\rho}(z)$ given by eq 6, to the simulation data.

$$\hat{\rho}(z) = \frac{1}{2}(\rho_l + \rho_v) - \frac{1}{2}(\rho_l - \rho_v)\tanh\left(\frac{2(z - z_e)}{w}\right) \tag{6}$$

https://dx.doi.org/10.1021/acs.langmuir.0c02243
Langmuir XXXX, XXX, XXX–XXX

The density profile $\hat{\rho}(z)$ is shown together with the simulation data in Figure S1 in the Supporting Information. The parameters ρ_l and ρ_v are the densities of the liquid and vapor phases, respectively, w is the thickness of the interface, and z_e is the position of the GDS.

We computed the wettability as a function of the interaction strength between the nanoparticle and the fluid particle, ε_{fn}, by performing simulations of a single nanoparticle on the interface. The nanoparticle was initially placed in the vapor phase and left to equilibrate and adsorb at the liquid−vapor interface for 10^3 steps. The wettability is defined the distance from the nanoparticle center-of-mass to the GDS of the liquid−vapor interface divided by the short radii of the nanoparticle l/b (see Figure 1). The wettability was calculated using trajectories over 5×10^5 steps and different ε_{fn}.

The interface deformation is the origin of the capillary forces between ellipsoidal nanoparticles adsorbed at interfaces. This was studied by equilibrating a nanoparticle at the interface for 10^3 time steps. Its orientation was fixed, while the local density of fluid particles was allowed to fluctuate. We calculated the local density in a surface layer around the nanoparticle. The layer was centered at the nanoparticle center, and it had a thickness equal to the short axis, b, of the nanoparticle. Averages were calculated over 5×10^5 steps.

The radial distribution function (RDF) was calculated for the tip and side of the ellipsoid, $g^{tip}(r)$ and $g^{side}(r)$, separately using

$$g(r) = \left\langle \frac{N(r, z)}{\hat{\rho}(z)} \right\rangle \frac{1}{V(r)} \tag{7}$$

where $N(r,z)$ is the number of particles a distance r away from the system origin and a position z relative to the liquid−vapor surface. The volume $V(r)$ is the volume of the shell, defined below for the tip and side of the ellipsoid separately. The ensemble average $\langle N(r,z)/\hat{\rho}(z)\rangle$ is computed by counting the particles in the volume $V(r)$. This local density is then weighted by the density profile of the liquid−vapor interface $\hat{\rho}(z)$, where z is the position of the counted particle relative to the liquid−vapor interface. The density profile is described by eq 6. We performed this weighted average to take into account the varying density of the fluid as we move from the liquid to the vapor phase. The density profile of the liquid−vapor interface was computed every time step. When the nanoparticle is fully submerged in the liquid or the vapor phase, the above weighting produces the standard RDF, where the normalizing density is that corresponding to the bulk liquid or vapor densities.

The volume $V(r)$ is defined as follows, for the tip, the RDF was calculated using spherical coordinates, (r, θ, φ). The origin of the spherical coordinate system used in calculating the RDF for the tip is a distance R away from the surface of the tip, where R is the radius of curvature of the ellipsoid at the tip

$$R = \frac{b^2}{a} \tag{8}$$

The advantage of this choice is that the spherical coordinate system exactly matches the curvature of the ellipsoid at the tip. The volume of a spherical sector shell of thickness $\Delta r = 0.043\sigma_0$ and polar angle $\theta \in [0,\pi/8]$ is

$$V^s(r) = 2\pi\left(1 - \cos\left(\frac{\pi}{8}\right)\right)\left(r^2\Delta r + \frac{\Delta r^3}{12}\right) \tag{9}$$

This volume is illustrated in Figure 4a.

At the side, the RDF is calculated using cylindrical coordinates, (r, φ, y). The origo of the coordinate system is the center-of-mass of the ellipsoid, the y-coordinate is oriented parallel to the long axis of the ellipsoid. The volume of the cylindrical sector shell of thickness $\Delta r = 0.043\sigma_0$, azimuth angle $\phi \in \left[-\frac{\pi}{8}, \frac{\pi}{8}\right]$, and length h is

$$V^c(r) = \frac{h\pi}{4} r\Delta r \tag{10}$$

This volume is illustrated in Figure 4b.

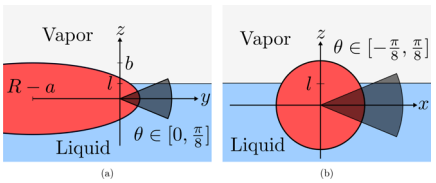

Figure 4. Systems used in the calculation of the radial distribution of the (a) tip and (b) side of the prolate ellipsoidal particle. $R = b^2/a$ is the radius of curvature at the tip of the nanoparticle, θ is the polar angle in the spherical coordinate system, ϕ is the azimuthal angle of the cylindrical coordinate system, l is the distance from the nanoparticle center-of-mass to the GDS of the liquid−vapor interface, and a and b are the long and short radii of the nanoparticle, respectively.

The solvent-mediated and capillary forces were computed by placing two nanoparticles, with a fixed separation d and orientation, in the vapor phase, as shown in Figure 1b,c. The nanoparticle pair did not rotate and it was set on a plane parallel to the liquid−vapor interface. The nanoparticle pair was left to equilibrate and adsorb at the interface for 10^3 steps. The solvent-mediated force was obtained for separations $d \in [0, 4\sigma_0]$, averaging over 5×10^5 steps, and using the equation

$$f(d) = \frac{1}{2}\langle \mathbf{r}_{ab} \cdot (\mathbf{f}_{af} - \mathbf{f}_{bf})\rangle \tag{11}$$

where the brackets represent a time average, $\mathbf{f}_{af}$ and $\mathbf{f}_{bf}$ are the total forces exerted by the fluid particles on the nanoparticle a and b, respectively, and $\mathbf{r}_{ab} = (\mathbf{r}_a - \mathbf{r}_b)/|\mathbf{r}_a - \mathbf{r}_b|$ is the unit vector along the axis between the centers of mass of the two nanoparticles.

RESULTS AND DISCUSSION

Interface Deformations. The interfacial deformation around prolate nanoparticles of radii $a = 7.5\sigma_0$, $b = c = 2.5\sigma_0$ and well depth ratios $\kappa' = 5$ and $\kappa' = 1$ was investigated by calculating the density of fluid particles around the nanoparticles and by calculating the RDF of fluid particles around the tip and side. The wettabilities for the two cases were $l/b = 0.63$ and $l/b = 0.65$ for the well depth ratios $\kappa' = 5$ and $\kappa' = 1$, respectively. These values correspond approximately to a contact angle $\theta = 51.0°$ and $\theta = 49.3°$, respectively. These wettabilities were chosen such that the interface deformations were maximized according to the work by Lehle *et al.*[5,21]

Figure 5 illustrates the density of fluid particles around the nanoparticles with well depth ratio (a) $\kappa' = 5$ and (b) $\kappa' = 1$. The view of the figures is normal to the liquid−vapor interface. The color scale in the figures indicates the fluid density ranging from $\rho^* = 0.5$ in dark blue to $\rho^* = 1.5$ in bright yellow. The color scale is cut, such that densities lower than $\rho^* = 0.5$ all give the same dark blue color.

The density of fluid particles around the nanoparticle with well depth ratio $\kappa' = 5$ is shown in Figure 5a. The interaction between the nanoparticle and the fluid is five times stronger at the side of the nanoparticle than at the tip of the nanoparticle. As a consequence, the density of fluid particles is higher at the sides of the ellipsoid as compared to the tips. We also found evidence for the formation of a coating layer of fluid around the nanoparticle center, as shown in Figure 6a. This effect is expected to reflect the experimental behavior because the generalized Gay−Berne model reproduced the anisotropic interaction arising from the shape of the nanoparticle.

The density after the first peak is lower at the tip compared to the side of the nanoparticle. This is clearly shown in the RDF shown in Figure 7a, and in the snapshot shown in Figure

https://dx.doi.org/10.1021/acs.langmuir.0c02243
Langmuir XXXX, XXX, XXX−XXX

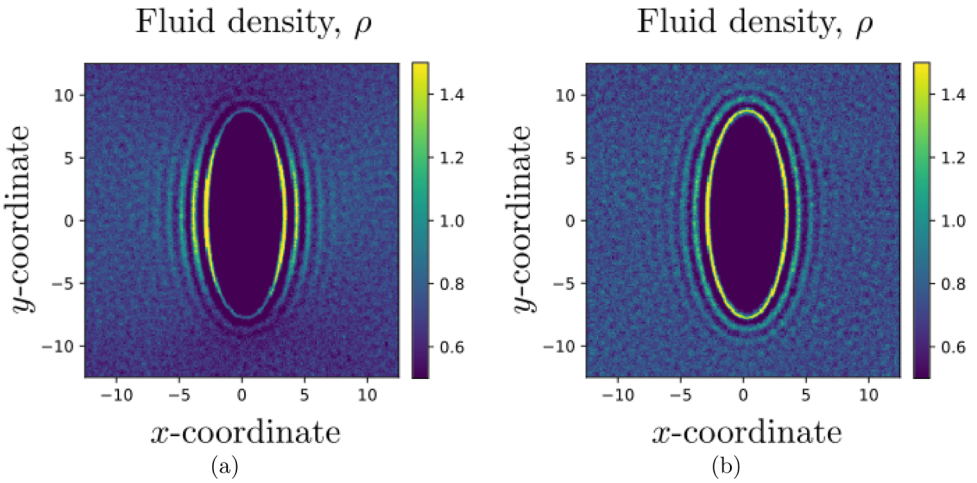

Figure 5. Density of fluid particles in a slab around a nanoparticle of radii $a = 7.5\sigma_0$, $b = c = 2.5\sigma_0$ adsorbed at the liquid−vapor interface. Well depth ratio and wettability (a) $\kappa' = 5$, $l/b = 0.63$ and (b) $\kappa' = 1$, $l/b = 0.65$.

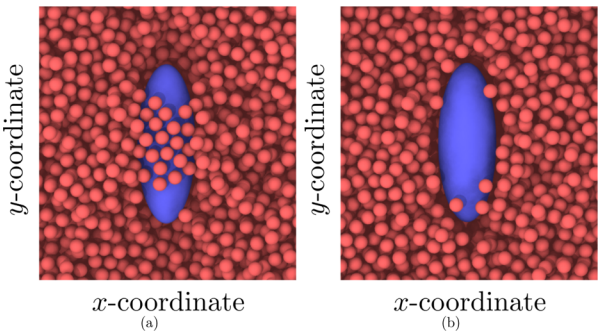

Figure 6. Snapshot of an ellipsoidal nanoparticle of radii $a = 7.5\sigma_0$, $b = c = 2.5\sigma_0$ adsorbed at a liquid−vapor interface with the well depth ratio and wettability (a) $\kappa' = 5$, $l/b = 0.63$ and (b) $\kappa' = 1$, $l/b = 0.65$.

6a. This is interpreted as a deformation of the liquid−vapor interface because of the presence of the nanoparticle.

To isolate the interfacial deformation effects from the interaction well depth ratio κ' and aspect ratio κ effects, we performed additional simulations using a depth ratio $\kappa' = 1$. We show in Figure 5b a top-down view of the density of the fluid around this nanoparticle. In this case, we do not see significant differences in the density of the fluid at the tip and sides of the nanoparticle (see Figure 5b). Following Lehle *et al.*,[5] we expect that the height of the meniscus associated with the fluid deformation around ellipsoids with aspect ratio $\kappa = 3$ and contact angle $\theta \approx 50°$ should be of the order $\Delta h \approx 0.18b = 0.45\sigma_0$. The interface deformation seen for the nanoparticle with well depth ratio $\kappa' = 5$ is concluded to be mainly due to the stronger interaction strength at the side than the tip, and not to the shape of the nanoparticle. The density profiles, as shown in Figure 5, show otherwise strong layering of the fluid around the nanoparticle. This is a significant effect that is not accounted for in continuum theory or finite element calculations. The layering is connected to the structuring of the fluid around the nanoparticle, which as we will see below, results in strong solvent-mediated forces.

The solvation structure around the nanoparticles can be examined in detail by analyzing the RDF. The RDF of the fluid particles around the tip and side of the nanoparticle of radii $a = 7.5\sigma_0$, $b = c = 2.5\sigma_0$, wettability $l/b = 0.63$, and well depth ratio $\kappa' = 5$ is shown in Figure 7a. The RDF is shown for the fluid structure around the tip (left panel) and the side (right panel) of the ellipsoidal nanoparticles separately. The RDF characterizes the packing of fluid particles close to the nanoparticle. The two graphs on the left show the radial distribution at the tip of the ellipsoidal nanoparticle and the two on the right show the distribution at the side of the nanoparticle. Close to the nanoparticle surface, there are two distinct peaks at the tip and five distinct peaks at the side. The same type of oscillations are also observed for fluid−solid surfaces with flat walls.[22] This means that there is a high degree of particle packing around the side of the nanoparticle and fewer fluid particles packing around the tip of the nanoparticle. Again, it is expected that this will give a high contribution to the solvent-mediated forces between two nanoparticles of this type because of this high degree of packing.

The first peak at the tip has a value 2.0 approximately at $r = 0.6\sigma_0$, while at the side the first peak has a value of 7.5 approximately at $r = 0.6\sigma_0$. This shows that the degree of fluid packing is much stronger at the side compared to the tip. Furthermore, the decay length of the solvation layers is significantly different reaching 2 and 4−5 fluid molecular diameters in the tip and side regions, respectively. This result indicates that the solvent-mediated forces can be strongly anisotropic in these systems.

The radial distribution of fluid particles around the tip and side of the nanoparticles of radii $a = 7.5\sigma_0$, $b = c = 2.5\sigma_0$, wettability $l/b = 0.65$, and well depth ratio $\kappa' = 1$ is shown in Figure 7b. At both the tip and the side of the nanoparticle, there are four distinct peaks. This means that there is a similar amount of packing around the tip as for the side of the nanoparticle. The first peak of the RDF at the tip and side has a value 4.2 approximately at $r = 0.6$.

Solvent-Mediated Forces. Figure 8 shows the solvent-mediated and capillary forces as a function of the surface-to-surface particle separation d for two spherical nanoparticles of radii $a = b = c = 2.5\sigma_0$. Three different cases were considered; nanoparticles completely submerged in the gas phase, completely submerged in the liquid phase, and adsorbed at the liquid−vapor interface. For the latter, the wettability is $l/b = -0.04 \pm 0.01$, corresponding to a contact angle of $\theta = 92.29 \pm 0.01°$. The bulk cases were calculated with a single gas or liquid phase. The interface case was calculated in a two-phase liquid−vapor system.

https://dx.doi.org/10.1021/acs.langmuir.0c02243
Langmuir XXXX, XXX, XXX−XXX

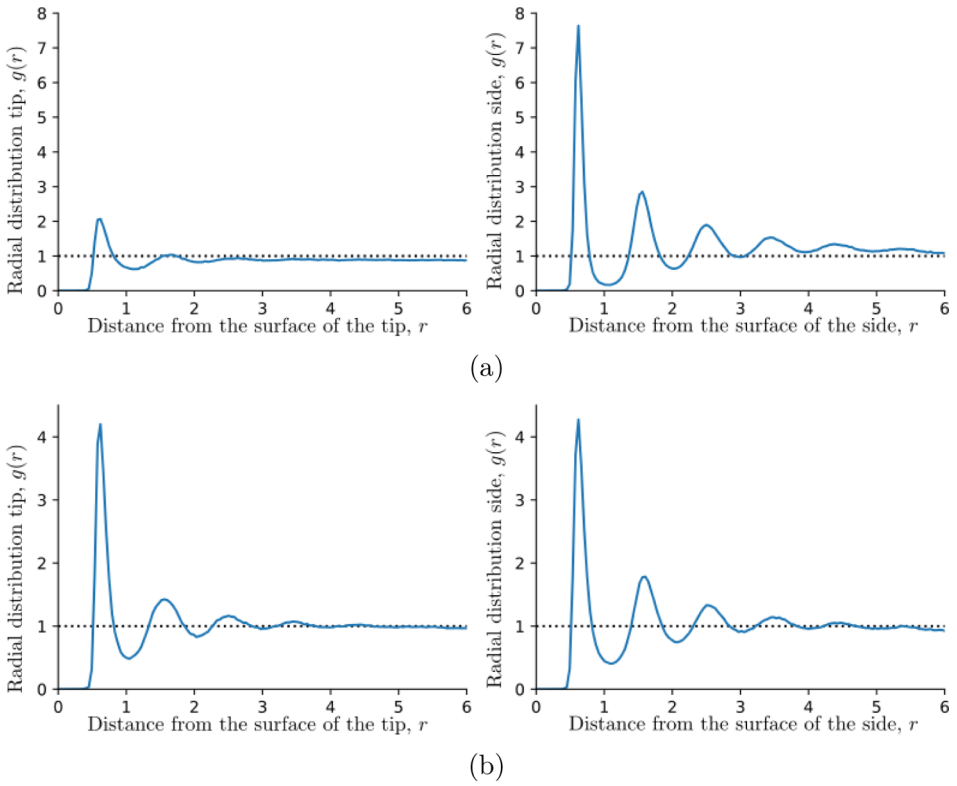

Figure 7. Radial distribution of fluid particles around the tip (left) and the side (right) of a nanoparticle of radii $a = 7.5\sigma_0$, $b = c = 2.5\sigma_0$. (a) Wettability $l/b = 0.65$ and well depth ratio $\kappa' = 5$. (b) Wettability $l/b = 0.63$ and well depth ratio $\kappa' = 1$. The reason why the RDFs in (a) are not exactly 1.0 for large r is that the surface is deformed up to distances beyond the range shown here, see Supporting Information.

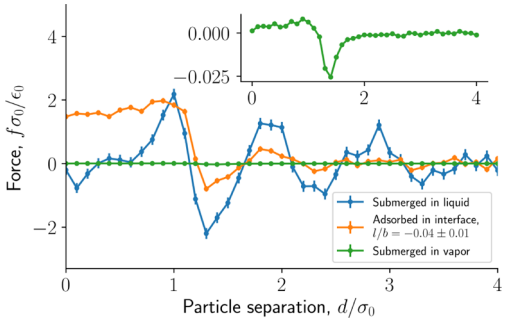

Figure 8. Solvent-mediated and capillary force acting between two spherical nanoparticles of radii $a = b = c = 2.5\sigma_0$ as a function of nanoparticle separation d. Submerged in liquid, vapor, and adsorbed at the liquid−vapor interface. The TT configuration is shown in the inset.

The force between nanoparticles exhibits oscillations that decay with increasing nanoparticle separation d for a separation larger than the fluid particle diameter $d > \sigma_0$. The oscillations have a period approximately equal the fluid particle diameter. These oscillations are caused by packing of fluid particles between the nanoparticles. They are larger for the nanoparticles submerged in the liquid phase and smaller for the nanoparticles adsorbed at the liquid−vapor interface, being essentially absent for the nanoparticle submerged in the vapor phase. These differences are correlated with the different densities of the liquid and vapor phases.

The depletion region is observed for separations smaller than the fluid particle diameter $d < \sigma_0$. For the nanoparticles adsorbed at the interface, the force is repulsive in the depletion region and for the nanoparticles submerged in the liquid phase, the force is decreasing as the separation decreases. The general behavior reported here agrees with previous studies of spherical particles adsorbed at interfaces.[9] These previous results show a larger solvent-mediated force in the vapor phase and the liquid phase. These differences are likely because the temperature and particle size were greater in the previous work, $T^* = 0.8$, $a = b = c = 3.5\sigma_0$. The additional repulsion for the forces between particles at the liquid−vapor interface is consistent with the results reported in ref 9. This extra repulsion was interpreted in that work in terms of a line tension term, which is only present when the nanoparticle is adsorbed at the liquid−vapor interface. The extra repulsion would arise from a negative line tension that pushes the particles apart in the depletion region, as the total line length is reduced when the total line length changes from two separate lines around each nanoparticle to a single line around both nanoparticles.

We have collected, as shown in Figure 9a, our results for the solvent-mediated and capillary forces between ellipsoidal particles of radii $a = 7.5\sigma_0$, $b = c = 2.5\sigma_0$ adsorbed at the liquid−vapor interface in three different orientations: SS, ST and, TT). The well depth ratio is $\kappa' = 5$, which corresponds to the interface deformation, as shown in Figure 5a, and RDF, as shown in Figure 7a, and theoretically gives a non-zero meniscus height $\Delta h \approx 0.45\sigma_0$ for a contact angle $\theta \approx 50°$[5] (see Figure 1a). The nanoparticle−fluid interaction parameter ϵ_{fp} is the same for the three different orientations. However, we point out that the wettability depends on the separation between the nanoparticles, d, and their relative orientation. This is because the local structure of the fluid particles depends on the orientation of the nanoparticles, which in turn changes the wettability. As a result, the wettability is not exactly the

https://dx.doi.org/10.1021/acs.langmuir.0c02243
Langmuir XXXX, XXX, XXX−XXX

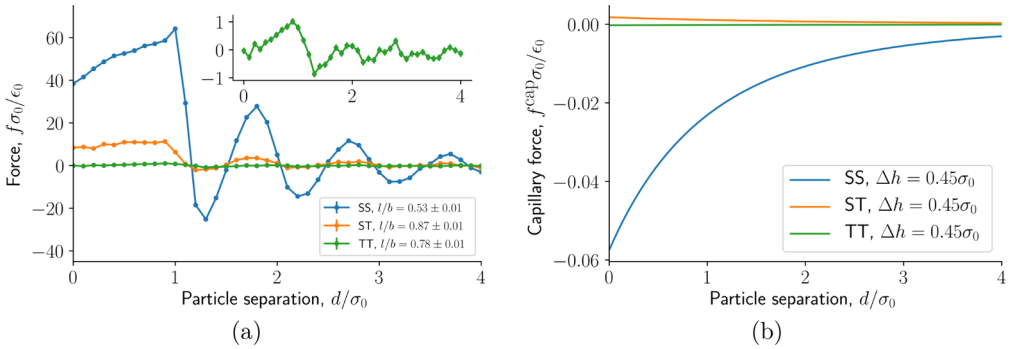

Figure 9. (a) Solvent-mediated and capillary force as a function of surface-to-surface separation d acting on a prolate nanoparticle with well depth ratio $\kappa' = 5$ for SS, ST, and TT orientations. The TT configuration is shown in the inset. (b) Capillary force f^{cap} as a function of surface-to-surface separation d, as described by eq 2, for a prolate nanoparticle of radii $a = 7.5\sigma_0$, $b = c = 2.5\sigma_0$ in the SS, ST, and TT orientations at the maximum expected meniscus height $\Delta h = 0.45$.

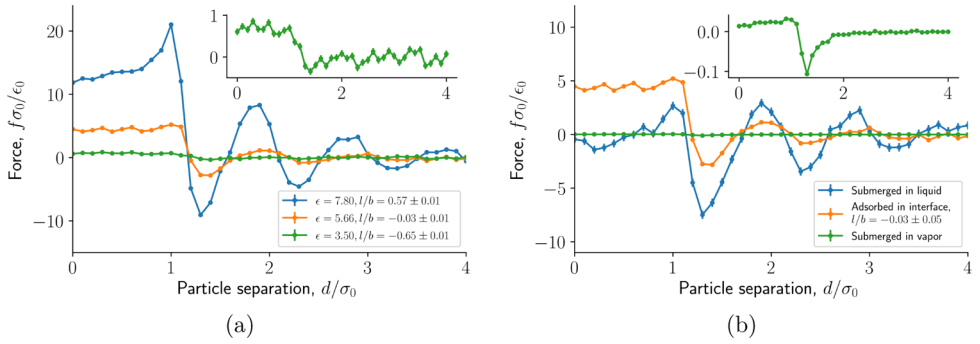

Figure 10. Solvent-mediated and capillary force as a function of surface-to-surface separation d acting on a prolate nanoparticle of radii $a = 7.5\sigma_0$, $b = c = 2.5\sigma_0$ and well depth ratio $\kappa' = 1$ in the SS orientation. (a) Adsorbed at the liquid−vapor interface with three different wettabilities. The lowest wettability is shown in the inset. (b) Same wettability in three cases, submerged in liquid, submerged in vapor, and adsorbed at the liquid−vapor interface. The vapor case is shown in the inset.

same for the three different cases. Equation 2 states that the capillary force in the SS and TT orientations is attractive and repulsive for the ST orientation for contact angles $\theta \neq 90°$.

Figure 9b shows the capillary force defined by eq 2, as a function of surface-to-surface separation in the SS and ST orientations with varying meniscus height Δh. The surface-to-surface separation d is $d = r - 2b$ and $d = r - a - b$ for the SS and ST orientations, respectively, where r is the center of mass to center of mass distance. This shows that the maximum capillary force that can be expected for particles of this size and wettability is of the order $f^{cap} = -0.06\frac{\sigma_0}{\epsilon_0}$, which is two orders of magnitude smaller than the total solvent-mediated forces calculated and presented in Figure 9a. Our results clearly show that the near field interactions (associated to solvent degrees of freedom) between small nanoparticles are determined mostly by solvent-mediated forces.

We show in Figure 10a the solvent-mediated and capillary forces between ellipsoidal particles of radii $a = 7.5\sigma_0$, $b = c = 2.5\sigma_0$ with well depth ratio $\kappa' = 1$ and three different wettabilities, $l/b = 0.57$, -0.03, -0.65 in the SS orientation. We did not find evidence for significant interfacial deformations in this system, see Figure 5b. The figure shows the same trend as the spherical particle, see Figure 8.

Finally, we show in Figure 10b the solvent-mediated and capillary forces between ellipsoidal particles of radii $a = 7.5\sigma_0$, $b = c = 2.5\sigma_0$ with well depth ratio $\kappa' = 1$ in the SS orientation. We have considered three different cases, submerged in liquid, submerged in vapor, and adsorbed at the liquid−vapor interface with wettability $l/b = -0.03$. The fluid−nanoparticle interaction parameters are the same for all three cases. The force outside the depletion region $d > \sigma_0$ oscillates with a period approximately equal to the fluid particle diameter. These oscillations are caused by the packing of fluid particles between the ellipsoidal nanoparticles. The force increases with the fluid particle density. This is equal to what we observe for the spherical particles, as shown in Figure 8. The force on the nanoparticles in the vapor phase is very small, this is because the fluid density is low, $\rho_v^* = (2.5 \pm 0.6) \times 10^{-4}$ compared to the liquid density $\rho_l^* = 0.7896 \pm 0.0004$.

Inside the depletion region $d < \sigma_0$, the force on the ellipsoidal nanoparticles adsorbed at the liquid−vapor interface is more repulsive than the nanoparticles submerged in the liquid phase, despite the larger fluid density in the liquid phase. This extra repulsion for the nanoparticle adsorbed at the liquid−vapor interface is caused by the liquid-vapor-nanoparticle three-phase line tension. The three-phase line tension is in this case negative and will act such that the nanoparticles are repelled. This is equal to what we observe for the spherical particles.

The repulsive force due to the line tension should be larger for neutrally wetting nanoparticles because the length of the three-phase line tension is at a maximum. However, this behavior is not observed inside the depletion region $d < \sigma_0$ for wettabilities $l/b = 0.57$ and -0.65 (see Figure 10a). We note that these data cannot be directly compared because the fluid−nanoparticle interaction parameters used in these two simulations are different. The liquid−nanoparticle and

https://dx.doi.org/10.1021/acs.langmuir.0c02243
Langmuir XXXX, XXX, XXX−XXX

vapor−nanoparticle surface tension and the liquid−vapor−nanoparticle line tension is expected to change with the interaction parameter. This is the reason why the nanoparticle with a lower contact angle has a higher repulsive force.

To assess the relevance of the depletion forces against direct nanoparticle−nanoparticle interactions, we performed additional simulations using a nanoparticle consisting of Lennard−Jones atoms, with the atoms interacting *via* the Lennard−Jones potential. We computed the forces between two prolate nanoparticles of radii $a = 7.19\sigma_0$ and $b = c = 2.53\sigma_0$ in vacuum. The diameters of the prolate nanoparticles are defined as the point where the nanoparticle−nanoparticle potential energy is zero. The potential well depth of the Lennard−Jones interaction is set to $\varepsilon_{np} = 0.7$. This interaction would be of the order of k_BT at 300 K; hence, similar to the interaction of methyl groups in aliphatic coatings used to passivate metallic nanoparticles.[23] We stress that other interactions are possible depending on the type of material but for comparison we consider here a representative energy scale used in experimental and modeling studies of small nanoparticles (see the Supporting Information for more details). The minimum nanoparticle−nanoparticle force reaches $f^{np}_{min} = -5.97\varepsilon_0/\sigma_0$ in the TT orientation and $f^{np}_{min} = -51.53\varepsilon_0/\sigma_0$ in the side-to-side orientation. The depletion force in the SS orientation for the case, as shown in Figure 9a, is of the same order of magnitude, highlighting the importance of solvent-mediated forces in determining near-field interactions between small nanoparticles. In the TT configuration, the depletion force is an order of magnitude smaller than the direct force. This result correlates well with the much smaller confinement effects associated with the TT orientation. The sum of the solvent-mediated, capillary, and direct force is presented in the Supporting Information.

CONCLUSIONS

A molecular dynamics simulation method to model prolate nanoparticles adsorbed at liquid−vapor interfaces has been established. This was done by modeling prolate nanoparticles with the Gay−Berne potential and fluid particles by the shifted and truncated Lennard−Jones potential. This has been used to study the interactions of prolate nanoparticles with interfaces and the interactions between prolate nanoparticles adsorbed at liquid−vapor interfaces.

It follows from the theory by Lehle *et al.*[5] that non-neutrally wetting prolate nanoparticles adsorbed at liquid−vapor interfaces, that is, with contact angles $\theta \neq 90°$ will deform the interface. A significant interfacial deformation was not found for prolate nanoparticles with well depth ratio $\kappa' = 1$. The expected interface deformation was approximately half the fluid diameter, which was too small to detect in our simulations. Theoretically, it has been predicted that such deformations introduce quadrupolar capillary interactions, which result in strong attractive or repulsive interactions for SS and tip-to-side relative orientations between particles. For the small nanoparticles, the small deformation would result in very small capillary forces, reaching a maximum of approximately $f^{cap} \approx -0.06\sigma_0/\varepsilon_0$ for the cases presented in this work. We have demonstrated that in near-field conditions other solvent-mediated forces, such as depletion interactions, are far more important than capillary forces.

We have examined using molecular dynamics simulations of Lennard−Jones and Gay−Berne models, the interactions between small nanoparticles, with characteristic sizes between 1 and 5 nm, that is, 3−5 solvent molecular diameters and aspect ratios 1−3. Our simulations show that at short interparticle separations (<1 nm) the interactions are dominated by solvent-mediated forces, which are between 10 and 10^3 orders of magnitude stronger than the quadrupolar interactions predicted theoretically using continuum models. This result shows that the interactions between small ellipsoidal nanoparticles are distinctively different from those predicted for large nanoparticles and cannot be described using a continuum approach that neglects the molecular nature of the solvent.

The solvent-mediated forces are strongly anisotropic and feature a longer range and strength when the particles are in a SS conformation. This effect is consistent with the existence of stronger layering of the solvent when it is confined between particles in this orientation. The solvent-mediated forces are weaker in the ST orientation reaching the smallest values for the TT orientation, which provides the smallest confinement effects.

Interestingly, we found that the forces in the depletion region are repulsive. Our investigation of ellipsoids in the corresponding bulk phases, liquid and vapor show that the repulsion is distinctively stronger when the particle is adsorbed at the interface. This result is consistent with a negative line tension, hence resembling the behavior observed in spherical particles adsorbed at liquid−vapor interfaces.[9]

We find that the depletion force in SS orientation is of the same order of magnitude as a characteristic nanoparticle-nanoparticle interaction of small nanoparticles coated with alkane layers in that orientation. The depletion force in the TT orientation is an order of magnitude smaller than the direct nanoparticle-nanoparticle interaction.

In order to observe clear evidence for capillary deformations, the simulation approach presented here may be used on larger nanoparticles, targeting larger aspect ratios κ. It is expected that the solvent-mediated force will decrease relative to the capillary force, which following the theory increases with the nanoparticle size.

ASSOCIATED CONTENT

Supporting Information

The Supporting Information is available free of charge at https://pubs.acs.org/doi/10.1021/acs.langmuir.0c02243.

Density profile $\rho(z)$, a calculation of the interface deformation and calculation of the direct nanoparticle−nanoparticle force; interface deformations have been calculated by calculating the GDS $z_e(x, y)$ in the plane normal to the liquid−vapor interface; and direct nanoparticle−nanoparticle force has been calculated by considering two atomistic nanoparticles of radii $a = 7.19\sigma_0$ and $b = c = 2.53\sigma_0$ constructed of Lennard−Jones atoms and calculating the force between them in vacuum (ZIP)

Solvation forces (PDF)

AUTHOR INFORMATION

Corresponding Author

Olav Galteland − *Department of Chemistry, Norwegian University of Science and Technology, Trondheim 7491, Norway;* orcid.org/0000-0002-6617-1377; Email: olav.galteland@ntnu.no

https://dx.doi.org/10.1021/acs.langmuir.0c02243
Langmuir XXXX, XXX, XXX−XXX

Authors

Fernando Bresme − *Department of Chemistry, Molecular Sciences Research Hub, Imperial College, London W12 0BZ, U.K.;* orcid.org/0000-0001-9496-4887

Bjørn Hafskjold − *Department of Chemistry, Norwegian University of Science and Technology, Trondheim 7491, Norway*

Complete contact information is available at: https://pubs.acs.org/10.1021/acs.langmuir.0c02243

Notes

The authors declare no competing financial interest.

■ ACKNOWLEDGMENTS

Computer resources have been provided by the Faculty of Natural Science at NTNU and by the HPC resources at UIT and NTNU provided by NOTUR, www.sigma2.no. O.G. and B.H. thank the Research Council of Norway through its Centers of Excellence funding scheme, project number 262644, PoreLab. F.B. would like to thank the Leverhulme Trust (grant no. RPG-2018-384) and the Imperial College High-Performance Computing Service for providing computational resources.

■ REFERENCES

(1) Bresme, F.; Oettel, M. Nanoparticles at fluid interfaces. *J. Phys.: Condens. Matter* **2007**, *19*, 413101.

(2) Rozynek, Z.; Mikkelsen, A.; Dommersnes, P.; Fossum, J. O. Electroformation of Janus and patchy capsules. *Nat. Commun.* **2014**, *5*, 3945.

(3) Dommersnes, P.; Rozynek, Z.; Mikkelsen, A.; Castberg, R.; Kjerstad, K.; Hersvik, K.; Fossum, J. O. Active structuring of colloidal armour on liquid drops. *Nat. Commun.* **2013**, *4*, 2066.

(4) Kralchevsky, P. A.; Nagayama, K. Capillary interactions between particles bound to interfaces, liquid films and biomembranes. *Adv. Colloid Interface Sci.* **2000**, *85*, 145−192.

(5) Lehle, H.; Noruzifar, E.; Oettel, M. Ellipsoidal particles at fluid interfaces. *Eur. Phys. J. E* **2008**, *26*, 151−160.

(6) Dasgupta, S.; Katava, M.; Faraj, M.; Auth, T.; Gompper, G. Capillary assembly of microscale ellipsoidal, cuboidal, and spherical particles at interfaces. *Langmuir* **2014**, *30*, 11873−11882.

(7) Loudet, J.-C.; Alsayed, A. M.; Zhang, J.; Yodh, A. G. Capillary interactions between anisotropic colloidal particles. *Phys. Rev. Lett* **2005**, *94*, 018301.

(8) Loudet, J. C.; Pouligny, B. How do mosquito eggs self-assemble on the water surface? *Eur. Phys. J. E* **2011**, *34*, 76.

(9) Bresme, F.; Lehle, H.; Oettel, M. Solvent-mediated interactions between nanoparticles at fluid interfaces. *J. Chem. Phys.* **2009**, *130*, 214711.

(10) Law, B. M.; McBride, S. P.; Wang, J. Y.; Wi, H. S.; Paneru, G.; Betelu, S.; Ushijima, B.; Takata, Y.; Flanders, B.; Bresme, F.; Matsubara, H.; Takiue, T.; Aratono, M. Line tension and its influence on droplets and particles at surfaces. *Prog. Surf. Sci.* **2017**, *92*, 1−39.

(11) Gay, J. G.; Berne, B. J. Modification of the overlap potential to mimic a linear site-site potential. *J. Chem. Phys.* **1981**, *74*, 3316−3319.

(12) Bresme, F. *Anisotropic Particle Assemblies*; Elsevier, 2018; pp 233−260.

(13) Wataru, S.; Shiga, M.; Mikami, M. Rapid estimation of elastic constants by molecular dynamics simulation under constant stress. *Phys. Rev. B: Condens. Matter Mater. Phys.* **2004**, *69* (13), 34103.

(14) Plimpton, S. Fast parallel algorithms for short-range molecular dynamics. *J. Comput. Phys.* **1995**, *117*, 1−19.

(15) Everaers, R.; Ejtehadi, M. Interaction potentials for soft and hard ellipsoids. *Phys. Rev. E: Stat., Nonlinear, Soft Matter Phys.* **2003**, *67*, 041710.

(16) Berardi, R.; Costantini, A.; Muccioli, L.; Orlandi, S.; Zannoni, C. A computer simulation study of the formation of liquid crystal nanodroplets from a homogeneous solution. *J. Chem. Phys.* **2007**, *126*, 044905.

(17) Brown, J. T.; Allen, M. P.; Martín del Río, E.; Miguel, E. d. Effects of elongation on the phase behavior of the Gay-Berne fluid. *Phys. Rev. E: Stat. Phys., Plasmas, Fluids, Relat. Interdiscip. Top.* **1998**, *57*, 6685.

(18) Babadi, M.; Everaers, R.; Ejtehadi, M. R. Coarse-grained interaction potentials for anisotropic molecules. *J. Chem. Phys.* **2006**, *124*, 174708.

(19) Trokhymchuk, A.; Alejandre, J. Computer simulations of liquid/vapor interface in Lennard-Jones fluids: Some questions and answers. *J. Chem. Phys.* **1999**, *111*, 8510−8523.

(20) Kirkwood, J. G.; Buff, F. P. The statistical mechanical theory of surface tension. *J. Chem. Phys.* **1949**, *17*, 338−343.

(21) Lehle, H.; Oettel, M.; Dietrich, S. Effective forces between colloids at interfaces induced by capillary wavelike fluctuations. *Europhys. Lett.* **2006**, *75*, 174.

(22) Evans, R.; Marini Bettolo Marconi, U. Phase equilibria and solvation forces for fluids confined between parallel walls. *J. Chem. Phys.* **1987**, *86*, 7138−7148.

(23) Reguera, J.; Ponomarev, E.; Geue, T.; Stellacci, F.; Bresme, F.; Moglianetti, M. Contact angle and adsorption energies of nanoparticles at the air−liquid interface determined by neutron reflectivity and molecular dynamics. *Nanoscale* **2015**, *7*, 5665−5673.